ACS APPLIED MATERIALS & INTERFACES

Research Article

www.acsami.org

Cobalt-Embedded Nitrogen Doped Carbon Nanotubes: A Bifunctional Catalyst for Oxygen Electrode Reactions in a Wide pH Range

Zilong Wang,[†] Shuang Xiao,[†] Zonglong Zhu,[†] Xia Long,[†] Xiaoli Zheng,[†] Xihong Lu,[‡] and Shihe Yang*[,†]

[†]Department of Chemistry, Hong Kong University of Science and Technology, Clear Water Bay, Kowloon, Hong Kong, China

[‡]School of Chemistry and Chemical Engineering, Sun Yat-Sen University, Guangzhou 510275, China

Supporting Information

ABSTRACT: Electrocatalysts for the oxygen reduction and evolution reactions (ORR/OER) are often functionally separated, meaning that they are only proficient at one of the tasks. Here we report a high-performance bifunctional catalyst for both ORR and OER in both alkaline and neutral media, which is made of cobalt-embedded nitrogen doped carbon nanotubes. In OER, it shows an overpotential of 200 mV in 0.1 M KOH and 300 mV in neutral media, while the current density reaches 50 mA cm^{-2} in alkaline media and 10 mA cm^{-2} in neutral media at overpotential of 300 mV. In ORR, it is on par with Pt/C in both alkaline and neutral media in terms of overpotential, but its stability is superior. Further study demonstrated that the high performance can be attributed to the coordination of N to Co and the concomitant structural defects arising from the transformation of cobalt-phthalocyanine precursor.

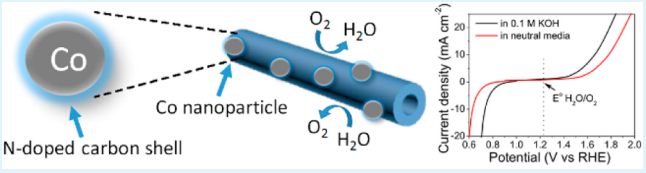

KEYWORDS: *bifunctional catalyst, carbon nanotube, cobalt-embedment, oxygen electrode reaction, wide pH range function*

INTRODUCTION

Increasing energy demands and environmental concerns have stimulated intense research on alternative energy conversion and storage systems aiming at high efficiency, low cost, and environmental benignity.[1] Fuel cells and metal−air batteries are desirable for future energy conversion and storage applications because of their theoretically high energy density. The oxygen reduction/evolution reactions (ORR/OER) play key roles in these devices.[2] The bottleneck of fuel cells mainly lies in the sluggish ORRs.[3,4] Traditional catalysts such as Pt and its alloys perform well, but the high cost limits their application. Thus, alternative catalysts based on nonprecious metals[2,5−8] or metal-free materials[9−11] have attracted much attention. As the reverse reaction of ORR, OER is at least equally important and underlies a battery of renewable energy technologies such as rechargeable metal−air batteries, water splitting, and solar fuel synthesis.[12−15] There have been some reports about OER catalysis using ruthenium and iridium oxides in alkaline conditions and first row spinel and perovskite metal oxides in basic conditions with moderate overpotentials.[16] However, most of them suffer from low activity because of the large particle size, low conductivity, and low specific surface areas. Even more challenging is to develop efficient bifunctional catalysts for both ORR and OER, which are especially useful for regenerative fuel cells, i.e., a water electrolyzer for the generation of the needed H_2 and O_2 products.[1,17]

At present, most OER/ORR bifunctional catalysts are prepared by combining separate ORR and OER catalysts into a composite. However, such simple physical mixing invariably leads to high electron transfer resistance. Some transition-metal oxides have structural and compositional semblance of the active center of the oxygen evolving complex, such as spinels, and thus show catalytic activity toward both OER and ORR.[18] However, again the performance is often impaired by their poor electronic conductivity. It has been established that the conductivity can be improved by doping with electron donors or by supporting on conducting materials, such as graphene/transition metal double hydroxide,[12,19,20] Mn_3O_4 with N-doped graphene,[21] and $NiCo_2O_4$ with N-doped graphene.[22] However, most of them can only work in either alkaline or acidic electrolytes but not neutral ones, even though neutral electrolytes are more useful for PEC water splitting due to their benign nature and low causticity.[23,24] Metal doping or embedding was found to be conducive to extending the catalytic environment from alkaline media to neutral media for HER and ORR owing to the cooperative and/or synergistic catalytic effects of the nanoparticles and the N dopants.[3,25] There have been some reports about using catalysts based on phthalocyanine and carbon materials as the oxygen electrode, which studied the metal−nitrogen bonding as active centers for the ORR and OER in alkaline media.[26,27] However, no studies have been reported on bifunctional catalysts based on metal embedded carbon material for the ORR and OER in a wide pH range. Catalysts of OER and HER, if working well in a common

Received: November 7, 2014
Accepted: February 4, 2015
Published: February 4, 2015

DOI: 10.1021/am507744y
ACS Appl. Mater. Interfaces 2015, 7, 4048−4055

pH range, could be coupled together to make the overall water splitting reaction more energy-efficient. However, most of the known HER catalysts work well only in neutral or acid media, whereas most of the known OER and ORR catalysts work well in alkaline media. Therefore, it is important and necessary to expand the working pH range of the OER and ORR catalysts. Most of the catalysts in alkaline and neutral media showed only one functional catalytic activity; e.g., they are either OER or ORR active but not both. In view of the need for bifunctional catalysts toward ORR and OER in a wide pH range for metal–air batteries and fuel cells, it is necessary to dope multiple components in a base catalyst such as carbon nanotubes. First of all, the composites based on carbon can ameliorate the catalyst degradation by hosting the active sites and reducing the electric resistance of metal oxide catalysts. Second, the dopant atom in carbon can also provide more active sites for ORR and OER. In the present work, we have designed and synthesized cobalt-embedded nitrogen doped carbon nanotubes (CNCNT) using cobalt-phthalocyanine (Co-Pc) as a precursor and the sources of cobalt and nitrogen. The CNCNT was studied as a bifunctional catalyst for ORR and OER in alkaline and neutral media. The catalyst was found to be especially suited for OER with a surprisingly high activity outperforming even noble (IrO_2) and some transition-metal catalysts such as Co_3O_4/N-rmGO,[1] NiFe LDH,[28] and Co_3O_4/mMWCNT.[23] As to ORR catalysis, it showed a comparable activity to a commercial carbon-supported Pt catalyst (20 wt % Pt on Vulcan XC-72, Pt/C) but with superior stability.

EXPERIMENTAL SECTION

Synthesis of the Cobalt-Embedded Nitrogen Doped Carbon Nanotubes. The steps of the synthesis are shown in Scheme 1. First, multiwalled carbon nanotubes (CNTs) (0.2 g) were dispersed in 50 mL of sulfuric acid (98%) by stirring for 1.5 h, followed by the addition of phosphoric acid (7 mL) under stirring for 20 min. At the same time, the mixture temperature was gradually increased to 70 °C. Solutions were then produced by the addition of 0.8 g of potassium permanganate at a rate of about 0.2 g per hour. The final mixtures were cooled to room temperature and then added into 300 mL of ice water containing H_2O_2 (10 mL; 30 wt %). The resulting solids were redispersed in deionized H_2O and dialyzed until the pH was close to 7. The solutions were further centrifuged at 7000 rpm for 30 min, followed by vigorous sonication for 15 min, and a mildly oxidized carbon nanotube product was obtained by freeze-drying. The oxidation step of carbon nanotube was intended to facilitate the reaction in the next step; it would activate more reaction sites to interact with Co-Pc.

Scheme 1. Synthesis of CNCNT[a]

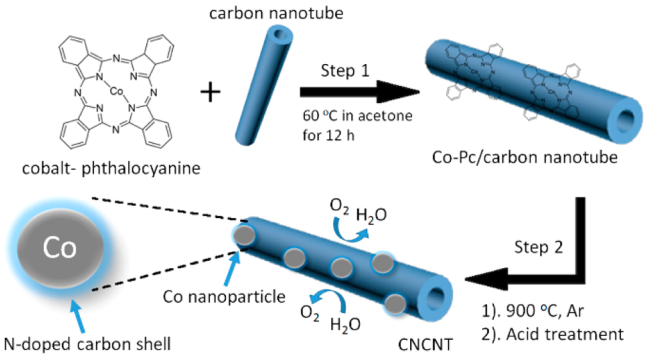

[a]Step 1: assembly of CoPc on carbon nanotubes in acetone at 60 °C for 12 h to form the precursor. Step 2: thermal treatment of the precursor at 900 °C in Ar atmosphere, followed by acid treatment to etch away any residual cobalt species.

Then, the carbon nanotube (50 mg) after 30 min ultrasonic treatment and cobalt-phthalocyanine (5, 10, 20, and 30 mg) were dispersed in 50 mL of acetone under ultrasonic treatment for 30 min. After that, the mixture was heated at 60 °C and refluxed for 12 h with stirring, followed by drying under vacuum at 60 °C. Through this step we obtained the CoPc-functionalized carbon nanotubes, which are the precursor for CNCNT. The CoPc-functionalized carbon nanotubes were then heated at 900 °C for 2 h in Ar, while the heating rate was 5 °C/min. The purpose of the heat treatment step was to incorporate the cobalt and nitrogen into the carbon nanotubes. Afterwards, the product was treated by 0.5 M H_2SO_4 for 24 h to remove any impurity and residual unembedded Co-Pc. The Co-Pc was replaced by $CoCl_2$ and phthalocyanine to prepare the CCNT. The NCNT was prepared in the same way, but the Co-Pc was replaced by phthalocyanine.

Characterization. The morphology and microstructures of the samples were investigated by HRTEM (JEOL-2010 with an acceleration voltage of 200 kV), SEM (JEOL-6700), and XRD (PW1830). The chemical composition was analyzed by XPS on PHI 5600.

Electrocatalytic Activity Evaluation. *Electrolytes Used.* The alkaline electrolyte is a 0.1 M solution of potassium hydroxide. The neutral medium is phosphate buffer solution prepared by K_2HPO_4/KH_2PO_4 (PBS, pH = 7), and the concentration is 1.0 M. The acid medium is a 0.5 M solution of sulfuric acid.

OER Activity Evaluation. The OER activity was evaluated using the catalysts loaded on Ni foam as the working electrode, coiled platinum wire as the counter electrode, and Ag/AgCl electrode as the reference electrode. The linear sweep voltammetry (LSV) scans were also performed using a CHI Electrochemical Station (model 660D) in a conventional three-electrode electrochemical cell at a scan rate of 10 mV/s and 0.1 mV/s for Tafel plots. Platinum wire and a Ag/AgCl, KCl (3 M) electrode were used as the counter and reference electrode, respectively.

ORR Activity Evaluation. The ORR activity was evaluated using a rotating disk (RRDE-3A). The LSV scans were performed using a CHI Electrochemical Station (model 660D) in a conventional three-electrode electrochemical cell at a scan rate of 10 mV/s. Platinum wire and an Ag/AgCl, KCl (3 M) electrode were used as the counter and reference electrode, respectively. We also used graphite rod as the counter electrode in ORR testing for comparison and found no significant difference (see Supporting Information Figure S9).

Preparation of Ni Electrode for OER. A 1 mg portion of catalyst was washed and dispersed in 0.967 mL of ethanol, and then 0.033 mL of 60 wt % PTFE was added into it. The mixture (containing 1 mg of catalyst) was under ultrasonic treatment for 10 min. After sonication for 1 h, 1000 μL of catalyst ink was drop dried onto a 1 cm × 1 cm Ni foam (loading 1 mg/cm^2). The Ni foam was washed with 0.5 M sulfuric acid, acetone, alcohol, and water successively to remove the metal oxide and any organics.

Preparation of Glassy Carbon Electrode for ORR. The preparation of a glassy carbon working electrode (5 mm in diameter) is as follows: prior to use the working electrode was polished mechanically with a 0.05 μm alumina slurry to obtain a mirror like surface, then washed with Mill-Q water and acetone, and allowed to dry. A 10 mg portion of the prepared NCN sample was dissolved in a 2 mL solvent mixture of Nafion (5 wt %) and alcohol (v/v ratio = 1:9) using sonication for 30 min and then 5 μL of the resulting electrocatalyst was dropped onto the glassy carbon electrode.

Number of Electrons Transferred. The number of electrons transferred (n) in the oxygen reduction reaction (ORR) was determined using the Koutecky–Levich (K–L) equation (eq 1)

$$1/J = 1/J_K + 1/J_L = 1/J_K + \omega^{-0.5}/B \quad (1)$$

where

$$B = 0.62nFC_0D_0^{2/3}\nu^{-1/6} \quad (2)$$

DOI: 10.1021/am507744y
ACS Appl. Mater. Interfaces 2015, 7, 4048–4055

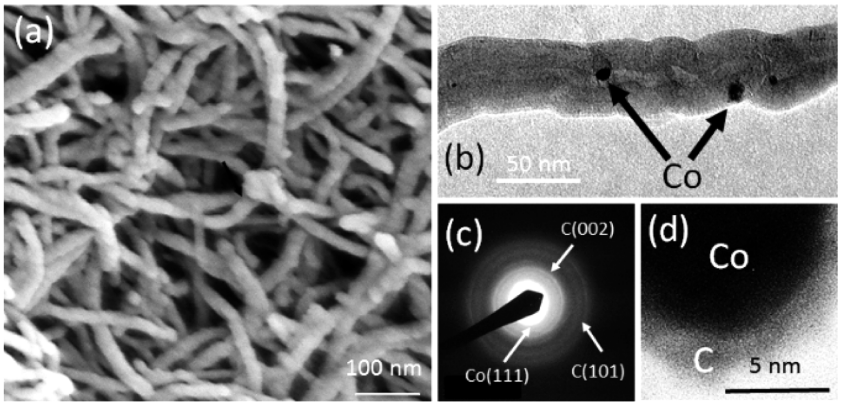

Figure 1. (a) SEM image of the CNCNT after acid treatment. (b) TEM image of a CNCNT. The arrows show the existence of cobalt nanoparticles. (c) Diffraction pattern of the carbon nanotube and the Co nanoparticles in part b. (d) TEM image of a single Co nanoparticle embedded in carbon nanotube and encased by N-doped carbon shell.

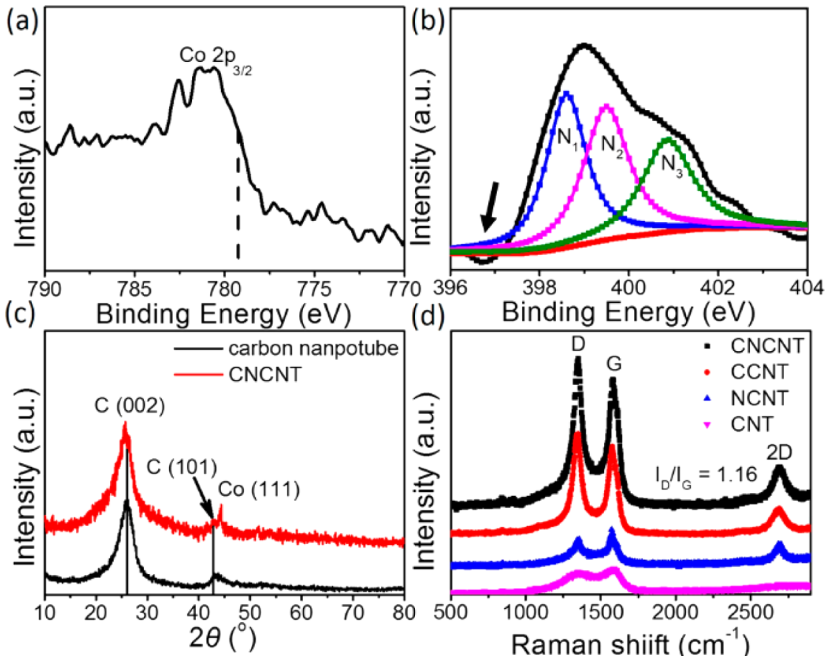

Figure 2. (a) Co 2p XPS spectrum of the CNCNT, the shoulder peak shows the Co−N moieties. (b) N 1s spectra of the CNCNT; N_1, N_2, and N_3 stand for the pyridinic, pyrrolic, and quaternary nitrogen atoms. (c) XRD patterns of the CNCNT showing the peaks of carbon nanotubes and cobalt nanoparticles. (d) Raman spectra of CNCNT: the I_D/I_G ratios of CNCNT, CCNT, NCNT, and CNT are 1.16, 1.1, 0.88, and 0.76, respectively.

$$J_k = nFkC_0 \quad (3)$$

where J_k is kinetic-limiting current density, J_L is diffusion-limiting current density, n is the overall number of transferred electrons during O_2 reduction, F is Faraday constant (96 500 C mol^{-1}), A is the geometric area of the electrode (cm^2), k is rate constant for oxygen reduction, C_0 is the saturated O_2 concentration in the electrolyte (1.2×10^{-3} mol L^{-1}), D_0 is the diffusion coefficient of O_2 in the electrolyte (1.9×10^{-5} cm^2 s^{-1}), ν is the kinematic viscosity of the solution (0.01 cm^2 s^{-1}), and ω is the angular frequency of the rotation in terms of rad s^{-1}.

RESULTS AND DISCUSSION

Scanning electron microscopy (SEM) images (Figure 1a) collected for the cobalt-embedded nitrogen doped carbon nanotubes using 10 mg CoPc (CNCNTs) show that the CNCNTs have a length of several micrometers and the thickness of the multiwalled carbon nanotube (MWCNT) is 20 nm. Transmission electron microscopy (TEM) images show some Co nanoparticles were embedded in the carbon nanotube (Figure 1b). The corresponding electron diffraction pattern of the CNCNT in Figure 1b is presented in Figure 1c, which shows the (002) and (101) planes of MWCNT and the (111) plane of Co nanoparticle. From the TEM image of a single Co nanoparticle in Figure 1d, we can find that the Co nanoparticle is about 7 nm in diameter and is encased by a 2 nm N-doped carbon shell. Note that the Co nanoparticles are quite inaccessible as they remain embedded within the nanotubes even after treatment with an acidic solution, which makes them stable in the catalytic reactions.

The X-ray diffraction (XRD) pattern in Figure 2c further confirms the existence of MWCNTs and Co nanoparticles. The peaks at about 26° and 42° correspond to the (002) and (101) planes of the MWCNTs, and the peak at 44° is assigned to the (111) of the Co nanoparticles.[25] The XRD result of the Co-Pc without carbon nanotube directly heated in Ar at 900 °C is shown in Supporting Information Figure S7, which is consistent

DOI: 10.1021/am507744y
ACS Appl. Mater. Interfaces 2015, 7, 4048−4055

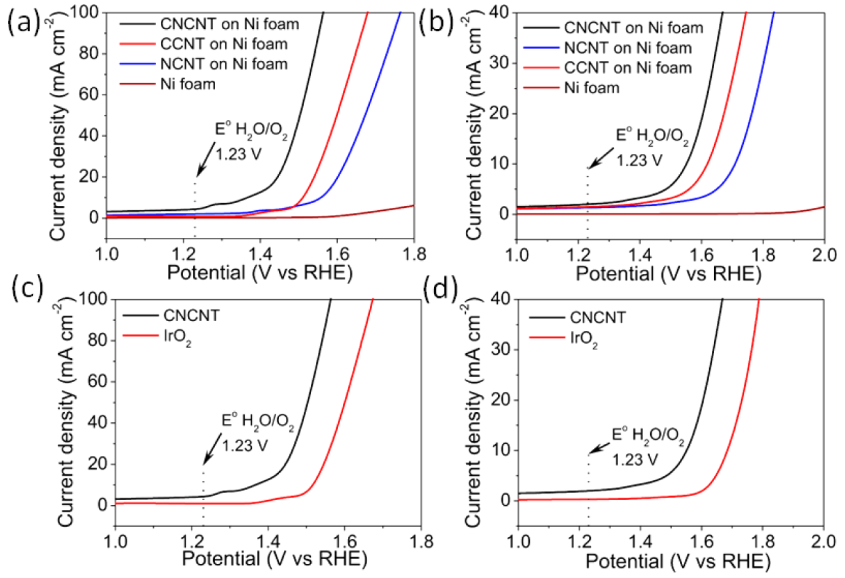

Figure 3. LSV plots recorded for CNCNT, CCNT, and NCNT supported on Ni electrode and a reference Ni foam electrode in 0.1 M KOH solution (a) and neutral media (b) at a scan rate of 10 mV s^{-1}; (c) LSV plots of CNCNT and IrO_2 in alkaline media; (d) LSV plots of CNCNT and IrO_2 in neutral media at a scan rate of 10 mV s^{-1}.

with the XRD result in Figure 2c. From this result we can confirm that the peak at 44° comes from the (111) of the Co nanoparticles. According to the X-ray photoelectron spectra (XPS) in Figure 2a,b and Supporting Information Figure S1, the Co/N atomic ratio is about 1:6, and the atomic content of Co is 0.22%. The peak of Co at about 782 eV is ascribed to metallic cobalt,[23] and the shoulder peak at about 778.8 eV can be assigned to the Co−N_x moieties, which support the existence of the coordination between Co and N (see Figure 2a).[25] The N 1s XPS spectrum of CNCNTs shown in Figure. 2b is mainly a convolution of three peaks associated with the common N−C structures, namely involving the pyridinic (398.6 eV), pyrrolic (400.3 eV), and quaternary (401.3 eV) nitrogen atoms, respectively. However, there is a low-binding-energy signal from 396 to 397 eV (indicated by an arrow in Figure 2b) that cannot be attributed to these three types of N−C structures. This result is consistent with the inference that the nitrogen atoms are coordinated to the Co nanoparticles.[26]

The Raman spectra shown in Figure. 2d display the characteristic D and G bands of the CNTs. The D band is due to the hybridized vibrational mode associated with the edges and defects of CNTs, while the G band is attributed to the tangential oscillation and vibration from all the sp^2 carbon atoms in the CNTs. Therefore, the intensity ratio of D and G bands (I_D/I_G) is often used to evaluate the defect density in carbon nanotubes. In this work, the I_D/I_G of the CNCNT is 1.2, which is higher than those of CCNT (1.1), NCNT (0.88), and CNT (0.76). This suggests that the use of Co-Pc as the cobalt and nitrogen source can bring more structural defects or microstructural rearrangement to the CNT. Plausibly, such defects from the N heteroatom and metallic Co nanoparticle can help to improve the catalytic performance of carbon nanotubes because of the enhanced π-bonding and electron donor−acceptor characteristics.[25]

The electrocatalytic activity of OER in alkaline and neutral media was evaluated using a typical three-electrode system, in which nickel foam modified with cobalt-embedded nitrogen doped carbon nanotubes was used as the working electrode, Ag/AgCl as the reference electrode, and platinum as the counter electrode. The evaluation of the ORR activity also used a similar three-electrode system except that the working electrode is changed to rotating disk electrode (RDE) modified with Co/N-doped carbon nanotubes.

First, the OER activity of CNCNT was investigated in alkaline media (0.1 M KOH) and phosphate buffer (1.0 M, pH = 7). We measured the quasisteady polarization curves in the alkaline (0.1 M KOH) and neutral media in the potential range 1−1.8 V (vs RHE) with a loading of 1 mg/cm^2 on Ni foam, and the result is shown in Figure 3a,b. In 0.1 M KOH, CNCNT shows high catalytic activity with smaller onset potential which is 1.43 V (vs RHE) (the overpotential is 200 mV), lower than those of the NCNT and CCNT. Also, the current increases quickly with the potential increase from 1.4 to 1.6 V (vs RHE). The overpotential is lower than those of metal oxide composite as well as carbon materials in the same alkaline media of 0.1 or 1 M KOH[1,12,28−33] (more data is shown in Supporting Information Table S1). The overpotential of OER catalyzed by CNCNT in neutral media is around 300 mV, larger than that in 0.1 M KOH, consistent with the previous studies. Moreover, this value is smaller than reported values obtained in the similar condition[23,34,35] (more data is shown in Supporting Information Table S2). What is more important is that the result in Supporting Information Table S2 shows that the performance of the CNCNT prepared in neutral media can reach the level of some materials in alkaline media. The current density of CNCNT is higher than that of the noble-metal catalyst (IrO_2, Figure 3c,d) in both alkaline and neutral media. We also tested the OER performance in acidic media, and the result is shown in Supporting Information Figure S8a. The catalytic performance did show some decrease in the acid media because of anion bonding to the active sites. Nevertheless, we have ascertained that the active pH range of our catalyst is quite wide.

From the LSV results shown in Figure 3a,b, it is worth noticing that, in 0.1 M KOH, the catalytic current of CNCNT reached 50 mA cm^{-2} at the overpotential of 300 mV, which is even higher than those of CCNT, NCNT, and other catalyst on Ni form.[1,12] Even in neutral media the catalytic current of

DOI: 10.1021/am507744y
ACS Appl. Mater. Interfaces 2015, 7, 4048−4055

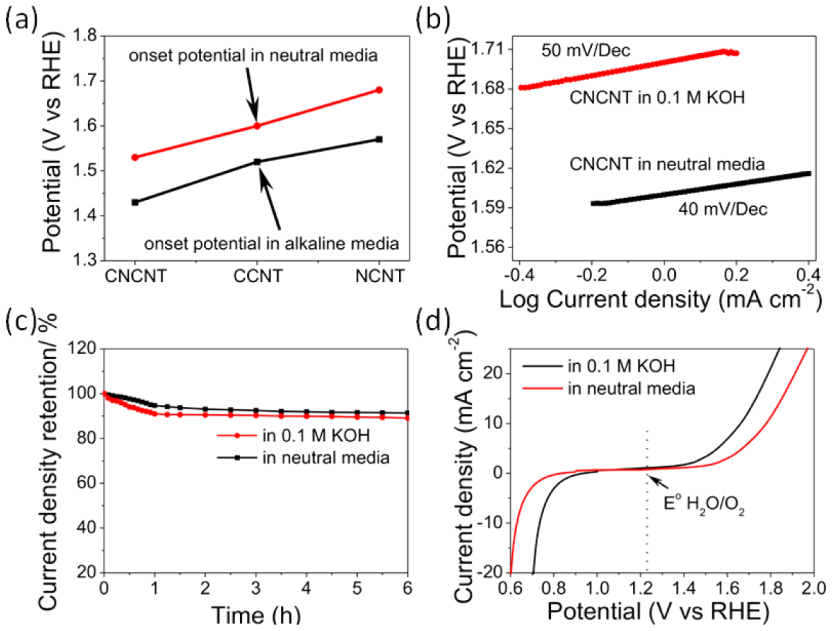

Figure 4. (a) Onset potentials of the OER catalyzed by prepared catalysts in alkaline and neutral media. (b) Tafel plots of CNCNT in alkaline and neutral media. (c) Chronoamperometric response of the CNCNT in alkaline and neutral media. (d) Oxygen electrode activities within the ORR and OER potential window of the CNCNT catalysts in oxygen saturated alkaline and neutral media (catalyst loading 1 mg cm^{-2} on Ni foam).

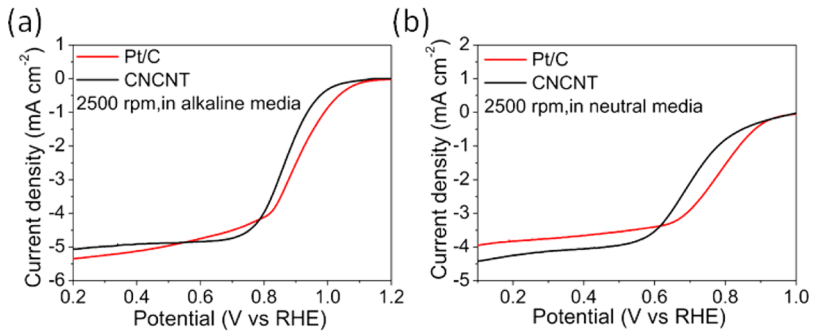

Figure 5. RDE voltammograms recorded for CNCNT and Pt/C supported on a GC electrode in an O_2-saturated 0.1 M KOH solution (a) and neutral media (b) at a scan rate of 10 mV s^{-1}.

CNCNT reached 10 mA cm^{-2} at the overpotential of 310 mV. The onset potentials of the different catalysts in alkaline and neutral media are shown in Figure 4a. Clearly, the Co-embedded nitrogen doped carbon nanotubes show a lower onset potential compared with the other modified carbon nanotubes such as CCNT and NCNT in the neutral and alkaline media.

The catalytic kinetics of CNCNT was further examined through Tafel plot shown in Figure 4b. The linear region is clearly observed on the Tafel plot, and its analysis according to the Tafel equation ($\eta = b \log j + a$, where η is overpotential, j is current density, and b is Tafel slope) yielded a much smaller Tafel slope value. The Tafel slope of CNCNT is 40 mV/Dec, which is much smaller than those reported previously.[1,12,21,28] When performed in neutral media the slope is 50 mV/Dec, which is again smaller than those reported in the literature.[36] Further experiments with CNCNT showed a very similar catalytic current in alkaline and neutral media as the scan rate was increased from 1 to 100 mV s^{-1} as shown in Supporting Information Figure S3a,b, due presumably to the highly efficient transport and favorable catalytic kinetics in the electrodes.[21]

To further test the stability performance of the CNCNT, we turned to the chronoamperometric method in the alkaline and neutral media. The potential we chose was 1.6 V versus RHE. Importantly, the CNCNT exhibits a high durability in alkaline and neutral electrolytes with less than 10% anodic current loss during 6 h of continuous potential cycles (Figure 4c), which is comparable with many reported carbon materials.[30,37] The stability in neutral media is somewhat better than in alkaline media because the carbon nanotubes suffer from degradation in alkaline media. The LSV plots of CNCNT after stability test are also collected, which is shown in Supporting Information Figure S4. The LSV results accord well with the result of the chronoamperometry results.

The low OER onset potential is likely due to the codoping of Co and N, the coordination between the codopants, and the concomitant structural defects, which account for the catalytic centers in the carbon nanotubes.[25,38]

In fact, the pyridinic and quaternary N atoms have proven to be the active sites for the OER and ORR because they can improve the electron donor−acceptor properties and enhance the π-bonding. The N atom here is special because on one hand, it has a high electronegativity, and on the other hand, its

DOI: 10.1021/am507744y
ACS Appl. Mater. Interfaces 2015, 7, 4048−4055

lone pair electrons can enhance the π-bonding. So the nitrogen dopants would enhance the bifunctional electrocatalytic performance.[25,39] Furthermore, the Co nanoparticles interact with nitrogen to form intimate bonds ($Co-N_x$),[3,26] also contributing to the improvement of the catalytic performance by generating more efficient catalytic active sites for ORR and OER.[40] In fact, it was shown previously that Co nanoparticles embedded in carbon nanotubes could lower the local work function of the carbon surface due to the facile electron transfer from the cobalt to the carbon.[25] The high stability is mainly attributed to the high conductivity of the carbon nanotubes with the doped nitrogen atoms and the embedded Co nanoparticles. The donor−acceptor properties promoted by the nitrogen dopants and the embedded Co nanoparticles would improve the conductance and interfacial electron transfer.[41] In addition, the Co nanoparticles are embedded in carbon so that they can be protected from leaching in the different media and kept robust for maintaining the stable catalytic reactions.[25]

Last, we extended the potential range of our hybrid electrode to 0.6 V (vs RHE) to evaluate the catalytic performance of ORR as is shown in Figure 4d. The CNCNT achieved an onset potential at about 0.8 V (in 0.1 M KOH, vs RHE) and 0.75 V (in neutral media, vs RHE), which shows a good catalytic performance for ORR. Furthermore, we tested the ORR performance in alkaline and neutral media using the LSV method; all of the tests were under the same condition with a loading of 0.1 mg/cm^2. Figure 5 shows the LSV result of ORR catalytic characteristics recorded on RDE loaded with CNCNT and Pt/C in alkaline media and neutral media. The LSV result in acid media is shown in Supporting Information Figure S8b. As shown in Figure 5a,b, the representative linear sweeping voltammetry of the CNCNT, measured on rotating disk electrodes (RDEs), showed an onset potential at about 0.9 V (vs RHE) in alkaline and 0.75 V (vs RHE) in neutral media. The gaps of the onset potential between the Pt/C and the CNCNT are less than 0.1 V in alkaline and neutral media. This gap shows the comparable performance with Pt/C in both of these media and better than some carbon based catalyst reported.[3,42,43] It is worth noticing that in neutral media the current density of CNCNT is higher than Pt/C catalyst after 0.7 V (vs RHE), and in alkaline media the current density is also close to Pt/C. These results attest to the ORR catalytic activity of CNCNT being comparable with that of Pt/C in both alkaline and neutral media, although the current density is not as high in acid media.

The LSV result has two regions of potential−current response. When scanning the potential cathodically, the currents increased rapidly in the mixed kinetic−diffusion control region and then slowed down, with the appearance of diffusion-limiting currents (I_d's).

Moreover, the current increased with rising rotational rates as a result of the faster oxygen flux to the electrode surface. The observed rotation-speed-dependent current I can be theoretically expressed by the Koutechky−Levich (K−L) equation for analyzing ORR kinetics (see Supporting Information).[44] The insets in Supporting Information Figure S5a,b show the constructed K−L curves, which plot $1/I$ versus $\omega^{-1/2}$ at 0.75, 0.8, 0.85, and 0.9 V in alkaline media (at 0.6, 0.65, 0.7, and 0.75 V in neutral media). The K−L plots in alkaline and neutral media exhibit good linearity, justifying the K−L analysis. The transferred electron number per oxygen molecule (n) in the ORR can be calculated from the slopes of the fitted linear line. The Lower n values indicate inferior performance. The calculated average electron-transfer number was about 3.9 in alkaline media and 3.7 in neutral media. Both of the numbers are less than the corresponding values with Pt/C (n = 3.99). These results suggest an apparent quasi-four-electron process in alkaline and neutral media, which is desirable for achieving high-efficiency electrocatalytic ORR.

To test the performance stability of our CNCNT in ORR, we performed chronoamperometry measurements, and the result is shown in Supporting Information Figure S6. Importantly, our CNCNT exhibits superior durability to Pt/C catalyst in both alkaline and neutral media, with 5% and 8% decay in ORR activity over 36 000 s of continuous operation. In comparison, the Pt/C exhibited 50% decrease both in alkaline and neutral media, giving lower long-term ORR currents than the stable currents sustained by the CNCNT. This comparable performance with Pt/C appears to stem from the embedded cobalt nanoparticles and the doped nitrogen atoms; that is, the special Co−N−C structure involving the pyridinic and quaternary N atoms works as the catalytic centers with superior catalytic performance.[3,39,40] Again, the better stability also comes from the high conductivity of carbon nanotubes with a unique 1D nanostructure, the N doping that improves the π-bonding and promotes the electron donor−acceptor activity, and the embedded Co nanoparticle.[39] These results vindicate our CNCNT as a powerful bifunctional catalyst for both oxygen reduction and water oxidation. Although some metal oxides and hybrid materials have shown bifunctional catalytic activities for ORR and OER,[1,2,17] our cobalt-embedded nitrogen doped catalyst stands out prominently with lower overpotentials for both ORR and OER, presenting excellent performance in a wide pH range as a novel nonprecious metal-based bifunctional catalyst.

CONCLUSIONS

In summary, we have successfully designed and prepared cobalt-embedded nitrogen doped carbon nanotubes for OER/ORR bifunctional catalysts using CoPc as the Co and nitrogen sources. This precursor pyrolysis method is particularly suitable for synthesizing novel catalysts such as the bifunctional catalyst in this report owing to its simplicity and controllability. The CNCNT shows an excellent catalytic performance for both OER and ORR not only in alkaline but also in neutral media. In OER it worked well with a small overpotential (200 mV in 0.1 M KOH and 300 mV in neutral media), low Tafel slope (40 mV/Dec in 0.1 M KOH and 50 mV/Dec in neutral media), and prominent electrochemical durability. Moreover, it also exhibited a quasi-four-electron process in catalyzing ORR with a comparable performance and higher stability compared with Pt/C in alkaline and neutral media. These outstanding performances are mainly attributed to a combination of the embedded cobalt and doped nitrogen, which can improve the stability and lower the overpotential. These results prove that the nanocomposite we prepared by precursor pyrolysis is among the best bifunctional catalysts for ORR and OER in both alkaline and neutral media. We anticipate applications of the electrocatalyst in, for example, bifunctional oxygen electrodes for metal−air batteries and regenerative fuel cells in both alkaline and neutral media.

DOI: 10.1021/am507744y
ACS Appl. Mater. Interfaces 2015, 7, 4048−4055

■ ASSOCIATED CONTENT

Supporting Information

XPS result of CNCNT and the LSV result of CNCNT catalyzing OER at different scan speed, after chronoamperometry test for 6 h. The LSV and stability result of CNCNT catalyzing ORR in alkaline and neutral media. Tables showing the performance of catalyst published for OER in alkaline and neutral media. This material is available free of charge via the Internet at http://pubs.acs.org.

■ AUTHOR INFORMATION

Corresponding Author

*E-mail: chsyang@ust.hk.

Notes

The authors declare no competing financial interest.

■ ACKNOWLEDGMENTS

This work was principally supported by HK-RGC General Research Funds (GRF No. HKUST 606511).

■ REFERENCES

(1) Liang, Y.; Li, Y.; Wang, H.; Zhou, J.; Wang, J.; Regier, T.; Dai, H. Co_3O_4 Nanocrystals on Graphene as a Synergistic Catalyst for Oxygen Reduction Reaction. *Nat. Mater.* **2011**, *10*, 780−786.

(2) Cheng, F.; Shen, J.; Peng, B.; Pan, Y.; Tao, Z.; Chen, J. Rapid Room-Temperature Synthesis of Nanocrystalline Spinels as Oxygen Reduction and Evolution Electrocatalysts. *Nat. Chem.* **2011**, *3*, 79−84.

(3) Zhao, Y.; Watanabe, K.; Hashimoto, K. Self-Supporting Oxygen Reduction Electrocatalysts Made from a Nitrogen-Rich Network Polymer. *J. Am. Chem. Soc.* **2012**, *134*, 19528−19531.

(4) Parvez, K.; Yang, S. B.; Hernandez, Y.; Winter, A.; Turchanin, A.; Feng, X. L.; Mullen, K. Nitrogen-Doped Graphene and Its Iron-Based Composite as Efficient Electrocatalysts for Oxygen Reduction Reaction. *ACS Nano* **2012**, *6*, 9541−9550.

(5) Zhu, H.; Zhang, S.; Huang, Y.-X.; Wu, L.; Sun, S. Monodisperse $M_xFe_{3-x}O_4$ (M = Fe, Cu, Co, Mn) Nanoparticles and Their Electrocatalysis for Oxygen Reduction Reaction. *Nano Lett.* **2013**, *13*, 2947−2951.

(6) Bashyam, R.; Zelenay, P. A Class of Non-Precious Metal Composite Catalysts for Fuel Cells. *Nature* **2006**, *443*, 63−66.

(7) Xiao, J.; Wan, L.; Wang, X.; Kuang, Q.; Dong, S.; Xiao, F.; Wang, S. Mesoporous Mn_3O_4-CoO Core-Shell Spheres Wrapped by Carbon Nanotubes: A High Performance Catalyst for the Oxygen Reduction Reaction and Co Oxidation. *J. Mater. Chem. A* **2014**, *2*, 3794−3800.

(8) Liang, J.; Zhou, R. F.; Chen, X. M.; Tang, Y. H.; Qiao, S. Z. Fe−N Decorated Hybrids of Cnts Grown on Hierarchically Porous Carbon for High-Performance Oxygen Reduction. *Adv. Mater.* **2014**, *26*, 6074−6079.

(9) Liang, J.; Du, X.; Gibson, C.; Du, X. W.; Qiao, S. Z. N-Doped Graphene Natively Grown on Hierarchical Ordered Porous Carbon for Enhanced Oxygen Reduction. *Adv. Mater.* **2013**, *25*, 6226−6231.

(10) Jin, J.; Pan, F.; Jiang, L.; Fu, X.; Liang, A.; Wei, Z.; Zhang, J.; Sun, G. Catalyst-Free Synthesis of Crumpled Boron and Nitrogen Co-Doped Graphite Layers with Tunable Bond Structure for Oxygen Reduction Reaction. *ACS Nano* **2014**, *8*, 3313−3321.

(11) Gong, K. P.; Du, F.; Xia, Z. H.; Durstock, M.; Dai, L. M. Nitrogen-Doped Carbon Nanotube Arrays with High Electrocatalytic Activity for Oxygen Reduction. *Science* **2009**, *323*, 760−764.

(12) Chen, S.; Duan, J.; Jaroniec, M.; Qiao, S. Z. Three-Dimensional N-Doped Graphene Hydrogel/NiCo Double Hydroxide Electrocatalysts for Highly Efficient Oxygen Evolution. *Angew. Chem., Int. Ed.* **2013**, *52*, 13567−13570.

(13) Suntivich, J.; May, K. J.; Gasteiger, H. A.; Goodenough, J. B.; Shao-Horn, Y. A Perovskite Oxide Optimized for Oxygen Evolution Catalysis from Molecular Orbital Principles. *Science* **2011**, *334*, 1383−1385.

(14) Nocera, D. G. Chemistry of Personalized Solar Energy. *Inorg. Chem.* **2009**, *48*, 10001−10017.

(15) Gong, M.; Li, Y. G.; Wang, H. L.; Liang, Y. Y.; Wu, J. Z.; Zhou, J. G.; Wang, J.; Regier, T.; Wei, F.; Dai, H. J. An Advanced Ni-Fe Layered Double Hydroxide Electrocatalyst for Water Oxidation. *J. Am. Chem. Soc.* **2013**, *135*, 8452−8455.

(16) Guerrini, E.; Chen, H.; Trasatti, S. Oxygen Evolution on Aged IrO_X /Ti Electrodes in Alkaline Solutions. *J. Solid State Electrochem.* **2007**, *11*, 939−945.

(17) Gorlin, Y.; Jaramillo, T. F. A Bifunctional Nonprecious Metal Catalyst for Oxygen Reduction and Water Oxidation. *J. Am. Chem. Soc.* **2010**, *132*, 13612−13614.

(18) Ma, T. Y.; Dai, S.; Jaroniec, M.; Qiao, S. Z. Metal−Organic Framework Derived Hybrid Co_3O_4-Carbon Porous Nanowire Arrays as Reversible Oxygen Evolution Electrodes. *J. Am. Chem. Soc.* **2014**, *136*, 13925−13931.

(19) Long, X.; Li, J. K.; Xiao, S.; Yan, K. Y.; Wang, Z. L.; Chen, H. N.; Yang, S. H. A Strongly Coupled Graphene and Feni Double Hydroxide Hybrid as an Excellent Electrocatalyst for the Oxygen Evolution Reaction. *Angew. Chem., Int. Ed.* **2014**, *53*, 7584−7588.

(20) Long, X.; Xiao, S.; Wang, Z. L.; Zheng, X. L.; Yang, S. H. Co Intake Mediated Formation of Ultrathin Nanosheets of Transition Metal LDH-an Advanced Electrocatalyst for Oxygen Evolution Reaction. *Chem. Commun.* **2015**, *51*, 1120−1123.

(21) Chen, S.; Duan, J.; Jaroniec, M.; Qiao, S.-Z. Nitrogen and Oxygen Dual-Doped Carbon Hydrogel Film as a Substrate-Free Electrode for Highly Efficient Oxygen Evolution Reaction. *Adv. Mater.* **2014**, *26*, 2925−2930.

(22) Chen, S.; Qiao, S.-Z. Hierarchically Porous Nitrogen-Doped Graphene−$NiCo_2O_4$ Hybrid Paper as an Advanced Electrocatalytic Water-Splitting Material. *ACS Nano* **2013**, *7*, 10190−10196.

(23) Lu, X.; Zhao, C. Highly Efficient and Robust Oxygen Evolution Catalysts Achieved by Anchoring Nanocrystalline Cobalt Oxides onto Mildly Oxidized Multiwalled Carbon Nanotubes. *J. Mater. Chem. A* **2013**, *1*, 12053−12059.

(24) Gerken, J. B.; McAlpin, J. G.; Chen, J. Y. C.; Rigsby, M. L.; Casey, W. H.; Britt, R. D.; Stahl, S. S. Electrochemical Water Oxidation with Cobalt-Based Electrocatalysts from pH 0−14: The Thermodynamic Basis for Catalyst Structure, Stability, and Activity. *J. Am. Chem. Soc.* **2011**, *133*, 14431−14442.

(25) Zou, X.; Huang, X.; Goswami, A.; Silva, R.; Sathe, B. R.; Mikmeková, E.; Asefa, T. Cobalt-Embedded Nitrogen-Rich Carbon Nanotubes Efficiently Catalyze Hydrogen Evolution Reaction at All pH Values. *Angew. Chem., Int. Ed.* **2014**, *53*, 4372−4376.

(26) Masa, J.; Xia, W.; Sinev, I.; Zhao, A.; Sun, Z.; Grützke, S.; Weide, P.; Muhler, M.; Schuhmann, W. Mn_xO_y/NC and Co_xO_y/NC Nanoparticles Embedded in a Nitrogen-Doped Carbon Matrix for High-Performance Bifunctional Oxygen Electrodes. *Angew. Chem., Int. Ed.* **2014**, *53*, 8508−8512.

(27) Zhu, Y.; Zhang, B.; Liu, X.; Wang, D.-W.; Su, D. S. Unravelling the Structure of Electrocatalytically Active Fe−N Complexes in Carbon for the Oxygen Reduction Reaction. *Angew. Chem., Int. Ed.* **2014**, *53*, 10673−10677.

(28) Lu, Z.; Xu, W.; Zhu, W.; Yang, Q.; Lei, X.; Liu, J.; Li, Y.; Sun, X.; Duan, X. Three-Dimensional NiFe Layered Double Hydroxide Film for High-Efficiency Oxygen Evolution Reaction. *Chem. Commun.* **2014**, *50*, 6479−6482.

(29) Gao, M.-R.; Cao, X.; Gao, Q.; Xu, Y.-F.; Zheng, Y.-R.; Jiang, J.; Yu, S.-H. Nitrogen-Doped Graphene Supported $CoSe_2$ Nanobelt Composite Catalyst for Efficient Water Oxidation. *ACS Nano* **2014**, *8*, 3970−3978.

(30) Wang, J.; Zhong, H. X.; Qin, Y. L.; Zhang, X. B. An Efficient Three-Dimensional Oxygen Evolution Electrode. *Angew. Chem., Int. Ed.* **2013**, *52*, 5248−5253.

(31) Landon, J.; Demeter, E.; İnoğlu, N.; Keturakis, C.; Wachs, I. E.; Vasić, R.; Frenkel, A. I.; Kitchin, J. R. Spectroscopic Characterization of Mixed Fe−Ni Oxide Electrocatalysts for the Oxygen Evolution Reaction in Alkaline Electrolytes. *ACS Catal.* **2012**, *2*, 1793−1801.

DOI: 10.1021/am507744y
ACS Appl. Mater. Interfaces 2015, 7, 4048−4055

(32) Liu, X.; Chang, Z.; Luo, L.; Xu, T.; Lei, X.; Liu, J.; Sun, X. Hierarchical $Zn_xCo_{3-x}O_4$ Nanoarrays with High Activity for Electrocatalytic Oxygen Evolution. *Chem. Mater.* **2014**, *26*, 1889−1895.
(33) Merrill, M. D.; Dougherty, R. C. Metal Oxide Catalysts for the Evolution of O_2 from H_2O. *J. Phys. Chem. C* **2008**, *112*, 3655−3666.
(34) Esswein, A. J.; Surendranath, Y.; Reece, S. Y.; Nocera, D. G. Highly Active Cobalt Phosphate and Borate Based Oxygen Evolving Catalysts Operating in Neutral and Natural Waters. *Energy Environ. Sci.* **2011**, *4*, 499−504.
(35) Mette, K.; Bergmann, A.; Tessonnier, J.-P.; Hävecker, M.; Yao, L.; Ressler, T.; Schlögl, R.; Strasser, P.; Behrens, M. Nanostructured Manganese Oxide Supported on Carbon Nanotubes for Electrocatalytic Water Splitting. *ChemCatChem* **2012**, *4*, 851−862.
(36) Irshad, A.; Munichandraiah, N. An Oxygen Evolution Co-Ac Catalyst—The Synergistic Effect of Phosphate Ions. *Phys. Chem. Chem. Phys.* **2014**, *16*, 5412−5422.
(37) Kadakia, K.; Datta, M. K.; Jampani, P. H.; Park, S. K.; Kumta, P. N. Novel F-Doped IrO_2 Oxygen Evolution Electrocatalyst for PEM Based Water Electrolysis. *J. Power Sources* **2013**, *222*, 313−317.
(38) Zhao, Y.; Nakamura, R.; Kamiya, K.; Nakanishi, S.; Hashimoto, K. Nitrogen-Doped Carbon Nanomaterials as Non-Metal Electrocatalysts for Water Oxidation. *Nat. Commun.* **2013**, *4*, 2390−2396.
(39) Ma, T. Y.; Dai, S.; Jaroniec, M.; Qiao, S. Z. Graphitic Carbon Nitride Nanosheet−Carbon Nanotube Three-Dimensional Porous Composites as High-Performance Oxygen Evolution Electrocatalysts. *Angew. Chem., Int. Ed.* **2014**, *53*, 7281−7285.
(40) Yu, H.; Li, Y.; Li, X.; Fan, L.; Yang, S. Electrochemical Preparation of N-Doped Cobalt Oxide Nanoparticles with High Electrocatalytic Activity for the Oxygen-Reduction Reaction. *Chem.—Eur. J.* **2014**, *20*, 3457−3462.
(41) Zheng, Y.; Jiao, Y.; Chen, J.; Liu, J.; Liang, J.; Du, A.; Zhang, W.; Zhu, Z.; Smith, S. C.; Jaroniec, M.; Lu, G. Q.; Qiao, S. Z. Nanoporous Graphitic-C_3N_4@Carbon Metal-Free Electrocatalysts for Highly Efficient Oxygen Reduction. *J. Am. Chem. Soc.* **2011**, *133*, 20116−20119.
(42) Zheng, Y.; Jiao, Y.; Ge, L.; Jaroniec, M.; Qiao, S. Z. Two-Step Boron and Nitrogen Doping in Graphene for Enhanced Synergistic Catalysis. *Angew. Chem., Int. Ed.* **2013**, *52*, 3110−3116.
(43) Tian, J.; Ning, R.; Liu, Q.; Asiri, A. M.; Al-Youbi, A. O.; Sun, X. Three-Dimensional Porous Supramolecular Architecture from Ultrathin G-C_3N_4 Nanosheets and Reduced Graphene Oxide: Solution Self-Assembly Construction and Application as a Highly Efficient Metal-Free Electrocatalyst for Oxygen Reduction Reaction. *ACS Appl. Mater. Interfaces* **2013**, *6*, 1011−1017.
(44) Yamamoto, K.; Imaoka, T.; Chun, W.-J.; Enoki, O.; Katoh, H.; Takenaga, M.; Sonoi, A. Size-Specific Catalytic Activity of Platinum Clusters Enhances Oxygen Reduction Reactions. *Nat. Chem.* **2009**, *1*, 397−402.

DOI: 10.1021/am507744y
ACS Appl. Mater. Interfaces 2015, 7, 4048−4055